RESEARCH ARTICLE

Hyper Spherical Search (HSS) Algorithm Based Optimization and Real-Time Stability Study of Tidal Energy Conversion System

ABHAY SANATAN SATAPATHY[1], **ASIT MOHANTY**[2,3], **(Senior Member, IEEE)**, **PRAKASH K. RAY**[4], **(Senior Member, IEEE)**, **JAVED KHAN BHUTTO**[5], **(Senior Member, IEEE)**, **AHMAD JABER MOHAMMAD ALFIAFI**[5], **AND OMAR KHULAIF ALHARBI**[5], **(Member, IEEE)**

[1]Faculty of Management Studies, Sri Sri University, Cuttack 754006, India
[2]Department of Electrical Engineering, MIET, Bhubaneswar 144411, India
[3]Division of Research and Development, Lovely Professional University, Phagwara, Punjab 144411, India
[4]School of Electrical Engineering, OUTR, Bhubaneswar 751003, India
[5]Department of Electrical Engineering, King Khalid University, Abha 62529, Saudi Arabia

Corresponding author: Asit Mohanty (amohanty@miet.edu.in)

ABSTRACT This article addresses the optimality and stability issues of a Tidal power based hybrid power system (HPS). The Tidal system gets destabilized by the uncertain variation of tidal waves and wind input. Stability of the system is restored through the introduction of Unified Power Flow Controller (UPFC) controller. The controller is optimized through the process of configuration of Hyper Spherical Search (HSS) based algorithm. The evaluation of the effectiveness of the suggested controllers is conducted through comparison analyses in order to regulate the voltage profile of the interconnected power network under various loading scenarios. The efficacy of the suggested controllers is assessed by stability analysis utilizing Eigen and Nyquist plots. Further, it is quite evident that optimal tuning is possible in case of the controller where the parameters can create significant impact on the system performance. Consequently, a novel heuristic optimization technique, such as HSS Algorithm are suggested to find the best output of the proposed controller. Finally, by using real-data, the performance as well as robustness of the suggested controller have examined by utilizing a real-time digital simulation platform, specifically the OPAL-RT 5142.

INDEX TERMS Direct drive permanent magnet synchronous generator, HSS algorithm, stability, reactive power compensation, unified power flow controller.

NOMENCLATURE

DG	Distributed generation.
HPS	Hybrid power system.
SG	Synchronous generator.
FACTS	Flexible AC transmission system.
ISE	Integral square error.
ITSE	Integral time multiplied square error.
Alpha	Phase angle.
RES	Renewable energy system.
AVR	Automatic voltage regulator.
IG	Induction generator.
PMSG	Permanent magnet synchronous generator.
ITAE	Integrated time multiplied absolute error.
IAE	Integral absolute error.
PM	Permanent magnet.
DDPMSG	Direct drive permanent magnet synch generator.
FACTS	Flexible AC transmission system.
DFIG	Doubly fed induction generator.
FPGA	Field-Programmable Gate Array.
PMIG	Permanent magnet induction generator.

SVC   Static var compensator.
UPFC   Unified power flow controller.
HSS   Hyper spherical search algorithm.
PWM   Pulse width modulation.
OF   Objective function.
GA   Genetic algorithm.
GWO   Grey wolf optimization.
P_{IG} Real power DFIG/DDPMSG.
Q_{DFIG} Reactive power DFIG.
P_{SG} Real power SG.
Q_{SG} Reactive power SG.
VSI   Voltage source inverter.
R_S Stator resistance.
PSO   Particle swarm optimization.
HSS   Hyper spherical search algorithm.
K_α, K_β Exciter gain, Gain of energy balance.
Q_{DDPMSG} Reactive power/DDPMSG.
T_α, T_r, T_S Exciter time const, rising time const, settling time const.
X_d Direct axis reactance of SG.
E_M Energy storage(DFIG).
ΔQ_{UPFC} Variation in Reactive Power.
Q_{IG} Reactive power IG.
ΔE_M Variation in change storage.
Q_{UPFC} Reactive power UPFC.
R_S Stator Resistance.
T_e, T_m Change in electromagnetic, mechanical torque.
ΔE_{fd} Change in voltage of Exciter.
CSI   Current source inverter.
$\Delta \alpha$ Change in phase angle.
ΔE_q Change in internal armature voltage.
L_s Stator Inductance.

I. INTRODUCTION

The deregulation of energy markets has resulted in the emergence of innovative renewable modular power producing technologies known as distributed generations (DGs). Renewable energy sources (RESs) exhibit unpredictable behavior in terms of power generation. Due to this rationale, the practicality of distributed generators (DGs) and conventional fossil fuel-powered electricity generation systems has prompted the emergence of a novel concept known as the hybrid power system (HPS).Distributed generation (DG) systems have demonstrated both economic and environmental benefits. Nevertheless, the presence of uncertainties in renewable energy sources (RESs) invariably impact various aspects of system performance, including power quality, stability, and reliability of the power system.

Tidal energy has recently gained prominence as a viable renewable energy source with the development of tidal power systems. The viability of utilizing tidal energy as an alternative energy source and the obstacles it presents are consistently formidable factors in the advancement of this technology. The utilization of hybridization or alternative
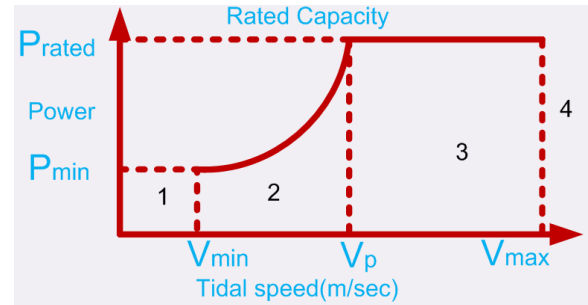

FIGURE 1. Power vs speed of a typical tidal power plant.

approaches to the wind energy system based on HPS technology near coastal areas can be observed. Moreover, the incorporation of the Tidal power plant into the primary grid system has garnered significant attention in recent decades. The integration of additional producing units, such as Tidal or Wind based power systems, into the current power network is a highly favorable progression.

The establishment of a correlation between power and tidal water speed is crucial in order to determine the appropriate control type, optimization strategies, or limitations. The power curve can be utilized in order to estimate the potential energy that can be harnessed from the approaching tide. Figure 1 illustrates an optimal power curve for a tidal turbine, whereby the cut-in and cut-out speeds represent the operational boundaries of the turbine. In addition, it is guaranteed that the energy level within this range remains above the minimum threshold in order to sustain the overall structural integrity. The rated power refers to the power recommended by the manufacturer, taking into account both energy and cost considerations.

The evolution of Tidal power generating technologies has been facilitated by the rapid advances in Tidal-based energy [1], [2]. In contemporary times, the DFIG and DDPMSG have gained extensive utilization in the domains of wind power and tidal-based energy sources due to their enhanced flexibility, improved efficiency, and notable adaptability [3], [4], [5]. Consequently, it is imperative to conduct an analysis to assess the influence of these two turbine types on system stability. DFIG based turbines use back to back converter in case of the rotor side circuit where the rotor fixes decoupling control in the stating. But it is noticed that DFIG based turbines make lots of losses due to the gear box problems. Therefore direct-drive permanent magnet generator (DDPMSG) is preferred as they have no gearboxes and require less maintenance. In case of DFIG based Tidal turbine the reactive as well as active power is managed through rotor current that is managed through the output voltage at the rotor portion converter. Further the dynamic responses of the Tidal turbine with DDPMSG are compared with DFIG.Custom power devices are widely used for stability improvement as well as reactive power management [1], [2]. In case of Tidal based HPS [3],stability improvement becomes very essential as the system often becomes unstable because of wide load variation

and uncertain nature of renewable resources. Uncertainty causes wide voltage deviation and creates unnecessary system parameter fluctuations [4], [5], [6], [7], [8].

Various control methods are employed for the management of controller design in Unified Power flow controllers (UPFC). The methods can be categorized into two distinct groups: classical controllers and current controllers. Within the realm of classical control techniques, such as Proportional-Integral (PI) controllers, it is possible to get the desired reference values for active and reactive powers, input bus voltage, and the internal variable of the DC capacitor voltage without resorting to the employment of UPFC dynamic equations. Despite being recognized as simple and practical techniques, PI controllers exhibit a lack of robustness at the operating point and can occasionally induce instability due to significant disturbances.

There have been numerous papers to improve the stability of DFIG based HPS with the help of UPFC.This paper suggests UPFC for improvement of stability [9], [10], [11] through compensating reactive power in DDPMSG based Tidal HPS [12], [13], [14].

Intelligent optimization techniques are always advocated for optimal design of the controllers [15], [16], [17], [18].In this regard this paper suggests HSS based algorithm [19], [20], [21] for obtaining optimal outcome [22], [23].The algorithm draws inspiration from the spherical spatial structure, wherein the population is comprised of two distinct groups: particles and centers of spheres. Each particle is assigned to one sphere space, goes toward the center of the sphere, and looks for the best center [24], [25], [26].The suggested method is evaluated against GA, PSO, and GWO in terms of its ability to discover the global minimum and its convergence speed. The simulation results support the usefulness of the suggested method and show that the HSS algorithm has faster convergence and results in a better solution than GA, PSO and GWO. In addition, the suggested HSS algorithm [26], [27] may be used as an alternate approach to solve optimization problems in varied domains of optimization problems, including industrial planning, resource allocation, scheduling, decision-making, pattern recognition and machine learning.

Authors of this present paper have used the efficacy of these optimization techniques in tuning the controller's gains involved with the tidal based HPS.The outcome yielded by these algorithms are compared with that of existing optimization techniques. Further the validation of the proposed control method in the linked power system is conducted using the OPAL-RT 5142 real-time digital simulation platform. The efficiency of the HSS [28], [29], [30] optimized PID controller is demonstrated through the comparison of simulation and real-time outcomes.

II. MATHEMATICAL MODELLING OF THE SYSTEM
Proposed tidal system composes of DFIG/DDPMSG based tidal turbine managed by SG based diesel generator having IEEE type-1 excitation system [Fig.1]. The Tidal based HPS
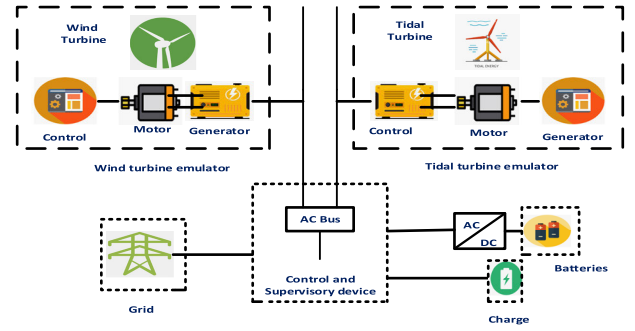

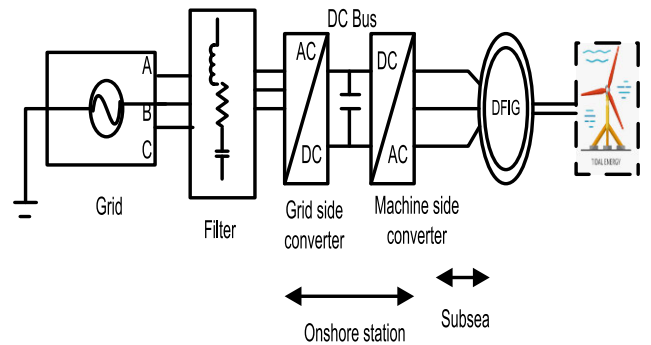**FIGURE 2.** Tidal energy based HPS set up.

FIGURE 3. Overview of tidal energy test system.

has been subjected to an incremental variation in loading that alters system parameters with a small magnitude and affects the control of reactive power inside the entire system. Small variation in the real power value affects the system's frequency while variable reactive power affects the system's terminal voltage.

Reactive power balanced equation of this Tidal based HPS

$$Q_{SG} + Q_{UPFC} = Q_L + Q_{DFIG/DDPMSG} \qquad (1)$$

With load variation ΔQ_L

$$\Delta Q_{SG} + \Delta Q_{UPFC} = \Delta Q_L + \Delta Q_{DFIG/DDPMSG} \qquad (2)$$

$$\Delta Q_{SG} + \Delta Q_{UPFC} - \Delta Q_L - \Delta Q_{DFIG/DDPMSG} = 0 \qquad (3)$$

The modified equation is

$$\Delta V(S) = \frac{K_V}{1 + ST_V} \left[\Delta Q_{SG}(S) + \Delta Q_{COM}(S) - \Delta Q_L(S) - \Delta Q_{DFIG/DDPMSG}(S) \right]$$

where $T_V = \frac{2H_r}{D_V} V^0$ and $K_V = \frac{1}{D_V}$

Typical small signal modelling [Fig.2,Fig.3]of the Tidal based HPS having the Tidal turbine with one induction generator (DFIG/DDPMSG),Diesel engine with a synchronous generator (SG) are connected to electrical loads is shown. Stability and reactive power management are achieved through custom power device like the UPFC.

The small signal modelling based SG equation is $Q_{SG} = \frac{\left(E'_q v \cos\delta - V^2 \right)}{X'_d}$ in transient condition
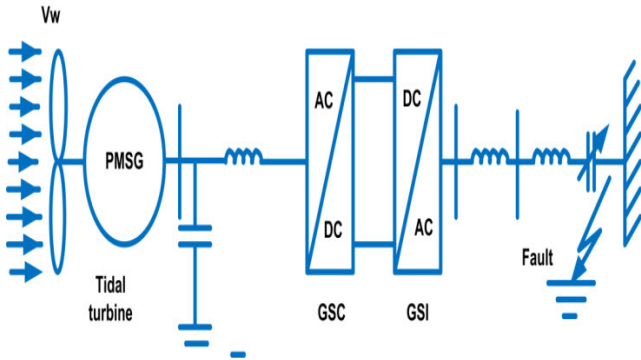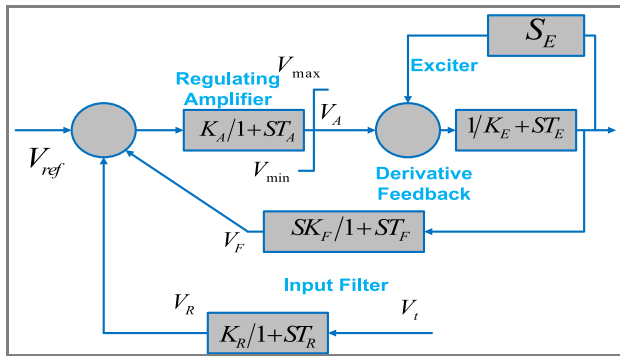
FIGURE 4. Tidal turbine model.

FIGURE 5. AVR model(IEEE-type1).

With incremental change

$$\Delta Q_{SG} = \frac{V \cos \delta}{X'd \Delta E'_q} + \frac{E'q\cos\delta - 2V}{X'd \Delta V} \qquad (4)$$

With the Laplace Equation the relation is

$$\Delta Q_{SG}(S) = K_a \Delta E'_q(S) + K_b \Delta V(S) \qquad (5)$$

$K_a = \frac{V\cos\delta}{X'd}$ and $K_b = \frac{E'_q\cos\delta - 2V}{X'd}$

The representation of the excitation system in literature often involves a single time constant high gain automatic voltage regulator (AVR).Among the various available AVR models, this particular isolated hybrid system employs the IEEE (type-I) AVR system as depicted in Fig. 4.

A. DFIG BASED TIDAL TURBINE

Single line DFIG block diagram has been shown in [Fig.6] where, the supply portion of this DFIG maintains the DC linked voltage continuous neglecting the orientation of the rotor power movement. Depending upon stator- flux vector positioning, the generator is managed through the synchronously revolving dq-axis frame. This active as well as reactive power management have been achieved through Iqr & Idr control near the rotor portion converter. Generally the diesel engine in the HPS manages active & reactive power in case of higher and variable loadings. Reactive power management in the output has been achieved through separate
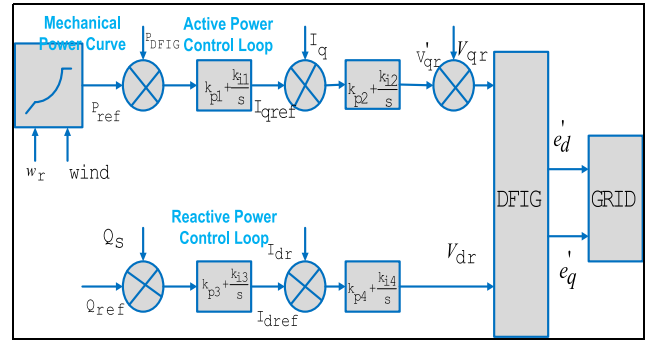
FIGURE 6. Control scheme of the rotor side PI controller of DFIG.

PI. Further the outer loop draws a comparison in between voltage related to DFIG with reference voltage.

$$Q_{DFIG} = \frac{L_m}{L_{SS}} V_1 I_{dr} - \frac{V_1^2}{w_s L_{ss}} \qquad (6)$$

The reactive power involved with DFIG as clearly represented in Fig. 5 is

$$\Delta Q_{DFIG}(s) = K_f \Delta I_{dr}(s) + K_e \Delta V(s) \qquad (7)$$

where $K_f = \frac{L_m V_1}{L_{SS}}$ and $K_e = \frac{L_m I_{dr}}{L_{SS}} - \frac{2V_1}{w_s L_{ss}}$

Here the rotor d -axis based reference current, and output signal in the voltage loop PI have been

$$\Delta I_{dr}^{ref} = \left(K_P + \frac{K_I}{s}\right)\left[\Delta V^{ref}(s) - \Delta V(s)\right] \qquad (8)$$

The dynamic inner loop is modelled as

$$\Delta I_{dr} = \frac{1}{\left(1 + \frac{t_s}{4}s\right)\Delta I_{dr}^{ref}}$$

$$\underline{X} = \left[\Delta I_{dr}^{ref}, \Delta I_{dr}, \Delta V, \Delta E_{fd}, \Delta V_a, \Delta V_f, \Delta E'_q\right]^T$$

$$\underline{U} = \left[\Delta V_{ref}\right]$$

$$\underline{w} = \left[\Delta Q_L\right]$$

B. DDPMSG BASED TIDAL TURBINE

In direct drive PMSG Tidal power system (DDPMSG)[Fig.6], the converter in the generator-side happens to be a rectifier while the grid portion converter remains as PWM type inverter[Fig.7]. These have been employed to get the desired dc bus voltage. Furthermore, it governs the power factor of the grid-portion by employing a decoupled d-q based vector controlling methodology. Furthermore, the dc-link serves to decouple the operation of converters.

DDPMSG functions like a SG(synchronous generator) having uniform rotor- flux linkage. From this equivalent circuit, standard equation for DDPMSG is mentioned as

$$L_S \frac{di_{ds}}{dt} = -V_{ds} - R_S i_{ds} + L_S w i_{qs} \qquad (9)$$

$$L_S \frac{di_{qs}}{dt} = -V_{qs} - R_S i_{qs} - L_S w i_{ds} + \omega\psi \qquad (10)$$
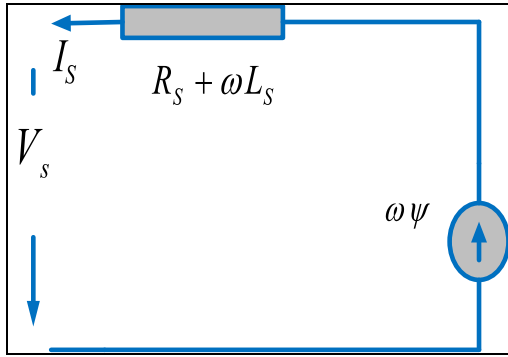
FIGURE 7. Equivalent circuit of DDPMSG model.

by aligning the direction of the d axis of the d-q reference frame with the flux linkage. Where v_{ds} represents director axis of the stator voltage while Vqs denotes the quadrature (q) axis in stator voltage. Additionally, the acronyms "Ids" and "Iqs" are used to represent the stator currents. The symbol Rs denotes the stator resistance, whereas Ls indicates the stator inductance. Additionally, the symbol ω is used to denote the speed of the generator. Thus Power equations have been derived as $P_S = V_{ds}i_{ds} + V_{qs}i_{qs}$ and $Q_S = V_{qs}i_{ds} + V_{ds}i_{qs}$ The generator side converter controls the active power of generator tracking the input of the Tidal turbine torque, and minimizes power losses of the generator. Further active power is governed through v_{qs} and power generator's power The minimization of loss is achieved by effectively managing the reduction of i_{ds} to zero. The implementation of control has been carried out utilizing the variable directivity system V_{ds}. Now the control equations have been as follows.

$$\dot{X} = f[x, z, u], Z = g[x, u]$$
$$X = [\omega_r, i_{ds}, i_{qs}, V_{dc}, X_1, X_2, X_3, X_4, X_5, X_6]^T$$
$$Z = [V_{ds}, V_{qs}, V_{dg}, V_{qg}]^T$$
$$U = [V_{d1}, V_{d2}, V_{d3}, V_{d4}]^T$$

X, Z, U are vectors linked to the state variables.

$$\Delta\dot{X} = A'\Delta X + B'Z + C'U \& \Delta Z = D'X + E'U \quad (11)$$

The converter situated at the Grid side sustains a consistent DC-linked voltage, as depicted in Figure 8, and influences the terminal voltage. The integration of reactive power management inside the Tidal-based HPS enhances the system's voltage stability. In the context of Tidal-based HPS, a control mechanism is employed to govern both the DC-link voltage and terminal voltage. This mechanism utilizes specialized techniques including the manipulation of certain variables $V_{Dg} \& V_{Qg}$.

$$V_{Dg} = K_{P5}\left(-K_{P3}\Delta V_{DC} + K_{i3}x_3 - iD_g\right)K_{i5x_5} + X_c i_{Qg} \quad (12)$$

$$V_{Qg} = K_{P5}\left(-K_{P4}\Delta V_t + K_{i4}x_5 - iQ_g\right)K_{i5x_6} + X_c i_{Dg} \quad (13)$$

K_{P5}, K_{i5} represent grid-converter gains. K_{P4}, K_{i4} represent terminal voltage regulation, K_{P3}, K_{i3} stand for the gains related to DC- bus voltage regulation.
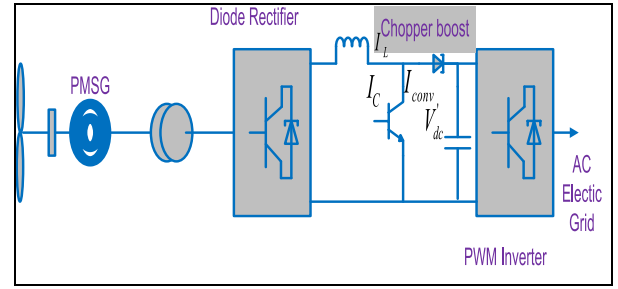

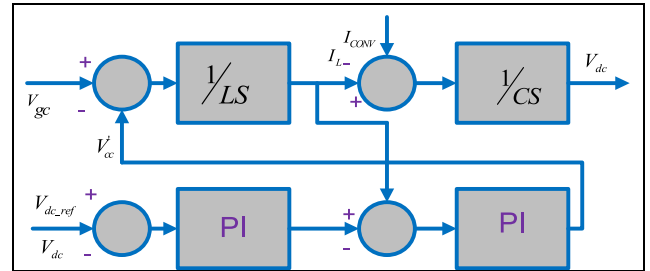**FIGURE 8.** Configuration of a PMSG based generator.

FIGURE 9. Control loop related to DC-linked voltage.

Here the combined system state matrix for the DDPMSG based tidal HPS can be formulated where,

$$\underline{X} = \left[\Delta\omega_t, \Delta i_{ds}, \Delta i_{qs}, \Delta V_{dc}, \Delta V, \Delta E_{fd}, \Delta V_a, \Delta V_f, \Delta E'_q\right]^T$$
$$\underline{U} = \left[\Delta V_{ref}\right]$$
$$\underline{w} = [\Delta Q_L]$$

For the Tidal based HPS with DDPMSG incorporated into power grid [Fig.9, Fig.10], system is modelled as

$$H\frac{dw_t}{dt} = T_M - T_e$$

$$T_M = \frac{0.5\rho\pi R^2 C_P V_W^3}{\omega_t}$$

where $C_P = \frac{1}{2}\left(\frac{RC_f}{\lambda} - 0.022\beta - 2\right)e^{-0.255(RC_f/\lambda)}$

$$T_e = -p\psi i_{qs}$$

C. UPFC CONTROLLER

UPFC Controller is one of the FACTS controller which helps in reactive power management and simultaneously increases the system voltage. UPFC composes of two VSIs with one source series and other source in parallel with that of the transmission line. It not only controls the reactive power but also controls the active power through injecting the AC voltage to the transmission line.

D. OPTIMISATION OF UPFC CONTROLLER

In any optimization technique application to a controller, objective function has been derived on desired specifications as well as constraints. Further the objective function helps in tuning the controller and is linked to performance index that takes care of the entire close loop. Output specifications

mainly compose of peak overshoots, steady-state Error, rising time and the settling time. The performance criteria taken into account in control design include the Integral of Squared Error (ISE), the Integral of Time multiplied Absolute Error (ITAE), the Integral of Time multiplied Squared Error (ITSE), and the Integral of Absolute Error (IAE). The commonest form of the performance criterion have been ISE and the ITAE criterions that show outstanding performances in comparison to IAE and ITSE.

Here performance indices such as ITAE have been considered that integrates all the absolute errors multiplied by time over a period of time. Further the tuning of this ITAE generates systems that settle rapidly than ISE based tuning. Here objective function has been expressed as

$$J = IATE = \int_0^\infty |\Delta V| \,.tdt$$

where ΔV indicates the system's voltage deviation. Problem constraints mentioned here are dependent on these control parameters. The optimization problem is realizable through minimization of objective function J in a range of $K_{I_{min}} \leq K_I \leq K_{I_{max}}$

$K_{I_{min}}$ and $K_{I_{max}}$ stand for the optimum values of control parameters.

III. HYPER SPHERICAL SEARCH (HSS) ALGORITHM

Similar to previous evolutionary algorithms, HSS algorithm commences by establishing an initial population. The population consists of two distinct categories of individuals, namely particles and hyper-sphere centers, which collectively constitute particle sets. The suggested evolutionary algorithm is founded on the exploration of the inner space of a hypersphere, which is created by the hyper-sphere core and its constituent particles. The HSS method is expected to converge to a state where a singular hyper-sphere center exists, and its constituent particles are positioned identically and possess equivalent cost function values to the hyper-sphere center. The application of the proposed approach exhibits its effectiveness in tackling a wide range of optimization difficulties by successfully optimizing several benchmark cost functions. The method being examined is assessed in relation to the GA,PSO, and GWO.The results suggest that the HSS algorithm demonstrates faster convergence and produces more optimal solutions in comparison to the GA, PSO, and GWO algorithms.

The utilization of the HSS algorithm in relation to a limited number of benchmark cost functions demonstrates its effectiveness in addressing various types of optimization tasks.

$$min \{f(x) | x \in X\}$$
$$\text{Subject to } g(x) \geq \text{ and } h(x) = 0$$

The application of the HSS method in conjunction with various benchmark cost functions demonstrates its effectiveness in addressing a wide range of optimization tasks.The objective of this optimization procedure is to minimize the

magnitude of objective function, denoted as f(x). In the realm of reality, each task is subject to varying degrees of limitations. The objective function (OF) is influenced by the sets of choice variables, which are constrained within the determined ranges of values as identified by variable X.

$$X_{i,min \leq} x_i \leq X_{i,max}$$

The algorithm technique in the novel consists of four distinct steps, namely:

The first step involves the initialization of particles.

Second Step: The Procedure of Conducting a Search

Third Step: Retrieval of dummy Particle

Step 4: Finding of the centers of new HSC as well as particles.

Step 5: Convergence Testing

The initialization process of the particle encompasses four distinct steps: (i) the process of initialization of parameter (ii) initial population and its generation (iii) the nomination of the hyper spheres, and (iv) the distribution of particles among the hyper spheres. Figures 3, 4, and 5 depict the spatial arrangement of particles, the progression of the dummy particle's retrieval process, and the flowchart outlining the High-Speed Sorting (HSS) procedure, respectively.

A.1. Initialization of parameter

The algorithm in question exhibits comparable parameters that are assigned by the user. The factors considered in this study are the initial population size N_{pop} and the number of HSCs.

A.2 Procedure for generating the initial population: In contrast to most standard evolutionary algorithms, the optimization process based on the (HSS) commences by randomly generating a group of individuals. Moreover, each variable x_i has been selected randomly from a distribution $[X_{i,min}, X_{i,max}]$ with a constant probability. In this particular instance, the answer has been designated as a particle, and the value of OF has been computed for each individual particle.

A.3. HSC nomination: In this particular instance, the particles are organized in a manner so that the OFVs are grouped in ascending way. In this study, a selection of the highest quality NSC particles has been made for the purpose of the HSC (SCs). In the context of N-dimensional optimization, particle is denoted by means of $1 \times N$ type vector, $[p1, p2, \cdots\cdots pN]$. *pi for i* $= 1, \cdots, N$ are having these decision variables. Further, OFV is determined after evaluation of the OF, f at $(p1, p2, \cdots pN)$ i.e., $f((p1, p2, \cdots pN))$.

A.4 The generation of particle circulation among a population of N particles in a HS's setting has occurred. Spherical shapes have been selected as the (SCs) in this study. The remaining particles have been allocated among the (SCs) while considering the dominance of SCs, which is inversely proportional to the objective function values (OFVs). To achieve a proportionate distribution of particles, an (OFD) has been designated for each (SC). The OFD is determined by calculating the difference between the OFV of a certain SC and the greatest OFV among all SCs.

Therefore, $OFD_{SC} = f_{SC} - max_{SCs}\{f\}$.

Further, the normalized dominance in each SC is defined as

$$D_{SC} = \left| \frac{OFD_{SC}}{\sum_{i=1}^{NSC} OFD_i} \right| K_\alpha, K_V \qquad (14)$$

So the primary number of these particles, which remains inside the SC, is equated to $\{D_{SC} \times (N_{pop} - N_{SC})\}$, taken up randomly through every SC among all particles remaining.

The search process is predicated on the notion that a particle will iteratively explore a confined space, delimited by a pre-established center, in order to discover an enhanced solution. Moreover, the variable 'r' represents the distance between the particles and the center of the sphere. The search method has been advanced by modifying the parameters in spherical coordinates, specifically the radial distance 'r' and the height 'h'. Fig.3 illustrates the representation of both the particle and the sphere within a three-dimensional setting. Moreover, it can be observed that in the context of an N-dimensional space, (N-1) angles appear in spherical coordinates for every individual point. In case of the N-dimensional space, it is observed that there are N-1 angles that exist, wherein the alteration of each angle contributes to the advancement of the particle within the seeking sphere. When considering the HSS, the particle undergoes a variation in its angle by one radian, with a corresponding probability $P_{r_{angle}}$. During each iteration procedure, a selection α is made randomly from a uniform distribution $(0, 2\pi)$. Following the introduction of angular variation, the distance between the center and the particle has been chosen in a random manner, with no specific constraints. When considering an N-dimensional hypersphere, the value of 'r' is determined between $[r_{min}, r_{max}]$ in the following manner.

$$r^2 = \sum_{i=1}^{N} \left(P_{i,center} - P_{i,particle} \right)^2$$

Upon the adjustment and evaluation of the variables θ_S and r the search process of the particle enters its completion phase. Throughout the search process, the spatial location of the particle undergoes alterations. Further, the parameters have been $r_{min}, r_{max}, P_{r_{angle}} \& SC$. In this context, individuals engage in the process of seeking HSs, taking into account both the (SC) and the operators that are specified by $Q[r_{min}, r_{max}, P_{r_{angle}} \& SC]$. Additionally, Following the particle seeking process within a sphere, it is possible for a particle to reach a point that exhibits a lower objective function (OF) value when compared to the associated (SC) value. In this scenario, there has been an interchange of labels between the SC and the particle, specifically, the newer SC still has the designation of being the particle. Moreover, this algorithm will advance its search by applying a novel search criterion at a more recent position.

A. RECOVERY OF THE DUMMY PARTICLES

During this period SC, combines with its corresponding counterpart to create a collection of particles. Amongst these particles, certain ones exhibit the highest magnitude of (OF), making it unfavorable for attending the global minimum level of OF. Meanwhile, these simulated particles inadvertently traverse unsuitable spatial regions. The process of doing a search in high school should be modified. In this particular stage, the aforementioned dummy particles are connected to different SCs, as illustrated in Fig.4. The aforementioned fact is represented by establishing the objective function value (OFV) of each set using the subsequent equation.

$$SOF = f_{SC} + \gamma \, mean \left\{ f_{particles \, of \, SC} \right\}$$

A decrease in the value of (SC) impacts the determination of the (SOF), whereas an increase in this value influences the positioning of the particles in the discovery of the SOF. Moreover, the value of 0.1 has been employed for the variable 'c' in the research article. The procedure for identifying the fake particle has been simulated by selecting certain dummy particles among the HSSs with the highest SOF and subsequently linking them to the other SCs. Furthermore, the distinction between each set can be effectively handled through the utilization of the under mentioned equation:

$$DSOF = SOF - max \, groups \{SOF \, of \, groups\}$$

The DSOF has been employed to allocate these particles to one of these SCs. Moreover, the determination of the AP of every SC is undertaken.

$$AP = \left| \frac{NTOF}{\sum_{i=1}^{NSC} NTOF_i} \right|$$

$$AP = [AP_1, AP_2, \cdots \cdots AP_{Nsc}]$$

A mechanism has been implemented to allocate the aforementioned particles among the (SCs). based on APs. Specifically, the dummy one is allocated to i-th SC having a certain probability. Ultimately, the group with the highest (SOF) is the one that relinquishes the dummy particle. Moreover, this particular phenomenon applies to the emerging subcategory within all SCs based on APs. Additionally, it is important to consider the implications of this phenomenon. It is worth noting that if a (SC) lacks any particles; it will undergo modification by acquiring a new particle and thereafter become a fresh SC through the use of a certain technique.

B. THE PROCESS OF IDENTIFYING AND CHARACTERIZING STEM CELLS (SCs) AND THE PARTICLES THAT MAKES UP THESE CELLS

As said earlier, particles that are examined within a spherical region have the potential to settle at a location where their magnitude is lower than the surrounding conditions they are associated with. Moreover, this occurrence has been visually represented following each search, with the specific location of the SC and the particles being interchanged. Moreover, in each iteration of the algorithm,

TABLE 1. Gain setting in the tidal based HPS for different controllers.

Tidal based HPS	Constant slip		Variable slip	
	K_P	K_i	K_P	K_i
DDPMSG(optimized)	34	5600	29	5661
DDPMSG (no controller)	46	7600	44	7791
DFIG	71	13500	60	13120
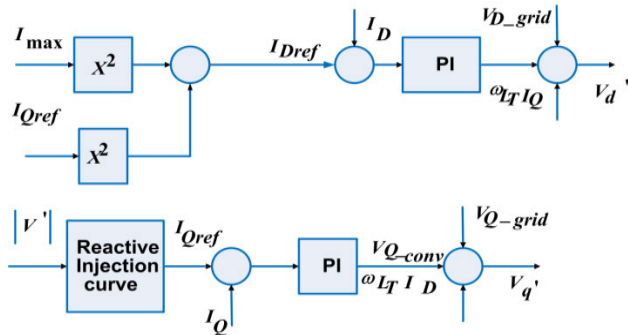
FIGURE 10. Grid-Side converter of tidal based HPS with DDPMSG.

TABLE 2. Results of the HSS based optimization in comparison to other tools.

Algorithm	K_P	K_i	K_d	M_p (%ge)	E_{ss}	t_r	t_s	J(pu)
GA	8.6121	3.4741	1.897	0.3439	0.0041	0.0343	0.1850	8.805
	6.3151	2.3431	1.2935	0.2974	0.0071	0.0390	0.2724	7.768
	5.6645	0.8275	1.958	0.1173	0.0097	0.1170	0.3608	6.765
CNC	1.9699	0.4947	0.2362	0.0111	0.0114	0.1779	0.2252	5.212
	1.9605	0.4922	0.2355	0.0109	0.0113	0.1816	0.1991	5.414
	1.9566	0.4893	0.2345	0.0104	0.0106	0.1961	0.5645	5.113
ABC	2.2835	0.6853	1.5532	0.0152	0.0045	0.1779	0.2262	5.745
	2.0204	0.5295	0.2497	0.0138	0.0092	0.1563	0.2135	5.202
	1.8749	0.452	0.2303	0.0129	0.0188	0.1651	0.2727	5.113
PSO	1.65	3.6987	0.3241	0.4670	0.0057	0.0316	0.2712	9.878
	2.5086	1.087	0.4093	0.0330	0.0164	0.1096	0.2303	6.277
	1.9102	0.4751	0.2291	0.0107	0.0116	0.1832	0.2211	5.3442
GWO	2.278	0.051	0.212	0.0121	0.0054	0.316	0.2015	5.16
	1.921	0.046	0.201	0.0105	0.0064	0.0668	0.182	5.12
	1.661	0.042	0.182	0.009	0.0082	0.102	0.180	5.10
HSS	2.032	0.038	0.183	0.011	0.007	0.313	0.177	4.342
	1.989	0.034	0.166	0.0102	0.0081	0.0548	0.170	4.221
	1.876	0.023	0.1567	0.0067	0.0084	0.0912	0.168	4.011

the (SCs) consistently exhibit reduced cost in terms of the objective function value (OFV) as compared to the particles within each set of particles. However, it is possible for a group of superconductors to contain one or more particles, resulting in these particles having a reduced cost in comparison to other superconductors. Furthermore, this particle demonstrates its superiority as a potential candidate for the space search algorithm in the subsequent iteration. Following each iteration, both particles and (SCs) have been arranged in ascending order based on their objective function (OF) values. The top-performing SCs have been identified and designated as newerSCs.Additionally; the remaining particles have been distributed across the aforementioned newer super clusters.
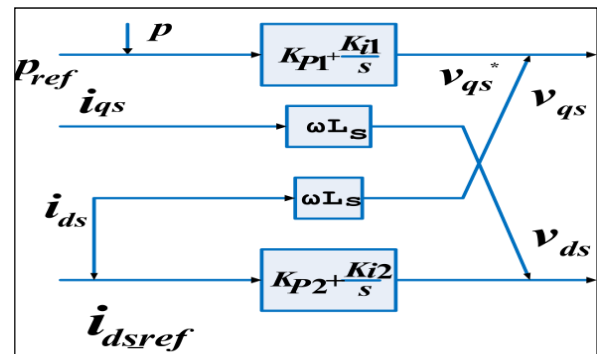
C. TEST OF CONVERGENCE

Following a certain duration, it is possible that all the SCs, with the exception of the highest quality ones, will be eradicated, then all the remaining particles are allocated to the superior SCs. In this scenario, there is no discernible distinction between the (SC) and all other particles. Moreover, all of these particles, along with the subject complement, exhibit comparable OF and occupy comparable positions. The functioning of the algorithm gets ended if any one of the under mentioned circumstances is reached.

In the event that the maximum number of iterations has been attained. If the percentage of change seen among the highest quality SCs in a series of consecutive iterations remains consistently below the predetermined threshold.
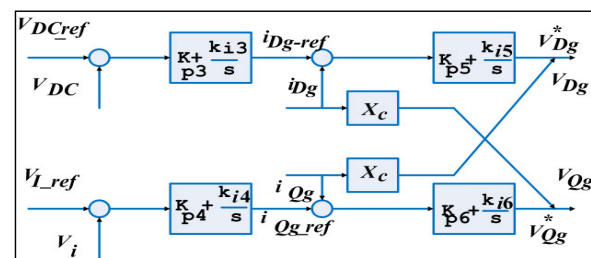
Fig.13 shows the convergence diagram (fitness value versus number of fitness evaluations). All the algorithms are testified for a particular number of fitness evaluations. These fitness evaluations have been chosen in order to

(a). Block diagram :Generator side

(b).Block diagram: Grid side

FIGURE 11. (a). Block diagram:Generator side . (b).Block diagram: Grid side.

find out which particular algorithm produces best fitness value. Because after that point the algorithms are not able to reduce further. The convergence graphs depicted in Fig.13 establishes that HSS algorithm is superior to
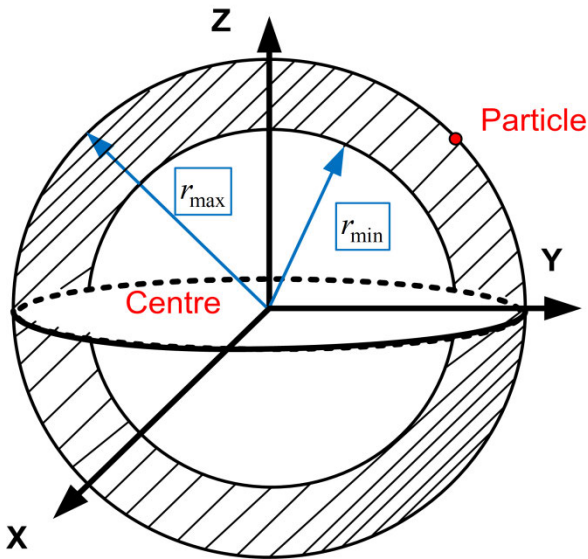
FIGURE 12. The likely location of the particle within a 3D, indicated by dashed lines.
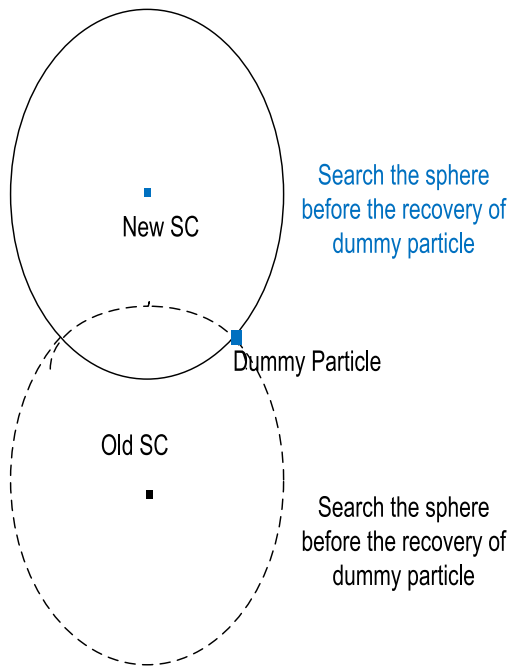

FIGURE 13. Recovery of the dummy particle.

TABLE 3. Damping factor and eigen values of the proposed HPS.

Tidal HPS (DFIG)			Tidal HPS (DDPMSG)		
Eigenvalue	Damping	Frequency	Eigenvalue	Damping	Frequency
-3.83e-2	1.00e+00	3.83e-02	-3.83e-02	1.00e+00	3.83e-02
-4.84e+00	1.00e+00	4.84e+00	-4.84e+00	1.00e+00	4.84e+00
-1.18e+1 + 3.06e+1i	3.59e-01	3.28e+01	-1.09e+1 + 3.06e+1i	3.36e-01	3.25e+01
-1.18e+1 - 3.06e+1i	3.59e-01	3.28e+01	-1.09e+1 + 3.06e+1i	3.36e-01	3.25e+01
-4.44e+01	1.00e+00	4.44e+01	-1.18e+1 + 3.06e+1i	3.59e-01	3.28e+01
-1.45e+02	1.00e+00	1.45e+02	-1.18e+1 + 3.06e+1i	3.59e-01	3.28e+01
-6.14e+02	1.00e+00	6.14e+02	-4.48e+1	1.00e+00	4.48e+01
-7.96e+04	1.00e+00	7.96e+04	-1.47e+2	1.00e+00	1.47e+02
			-6.18e+2	1.00e+00	6.18e+02
			-7.99e+4	1.00e+00	6.18e+02

IV. SIMULATION AND RESULTS

A comparative analysis has been conducted to assess the transient responses of DFIG and DDPMSG based Tidal turbines. Such as UPFC.Optimised outcome have been studied with GWO, GA, PSO and HSS algorithms based UPFC Controller. During observation it is noticed that transient responses in case of DDPMSG with UPFC exhibits better damping than DFIG based Tidal HPS. DDPMSG based HPS's performance has been further improved through HSS based algorithm. It can be inferred that the transient responses in case of DDPMSG based Tidal HPS with UPFC is better than DFIG based system.

Transient responses for 5% step load increase in the Tidal Turbine based HPS with UPFC is presented in [Fig.13 (a-f)]. It is noticed that for facing the mismatch of reactive power during transient, reduction in the size of UPFC and Tidal power generating unit require higher gain to offset. Terminal voltage's peak value variation occurs in accordance with the sizing of the Tidal turbine. Results of HSS based optimization [Fig.12] have been compared with other techniques [Table.2].

Optimum gains of the PI and PID in UPFC based DDPMSG have been tuned having 5% step increase in load and tidal power. Optimum values for Tidal based HPS have been shown. Optimized values have been determined with the application of HSS optimization based UPFC. During observation, peak values of the voltage deviation along with settling time vary with the reduction in the dimension of DFIG/DDPMSG based turbine [15(a-g), 16(a-e)].

A. STABILITY ANALYSIS

In addition, the stability study of the Tidal-based Hydro-electric Power System (HPS) with Doubly Fed Induction Generator (DFIG) and Direct-Drive Permanent Magnet Synchronous Generator (DDPMSG) has been examined using various analytical tools, including Bode plots, Nyquist plots, circle criterion, and Popov criterion, as illustrated in Fig.17 (a-e). The Nyquist stability criterion postulates that a system will achieve stability when the feedback gain, represented as k, satisfies the condition that the point -1/K does not lie in the right half-plane of the stability plane. The
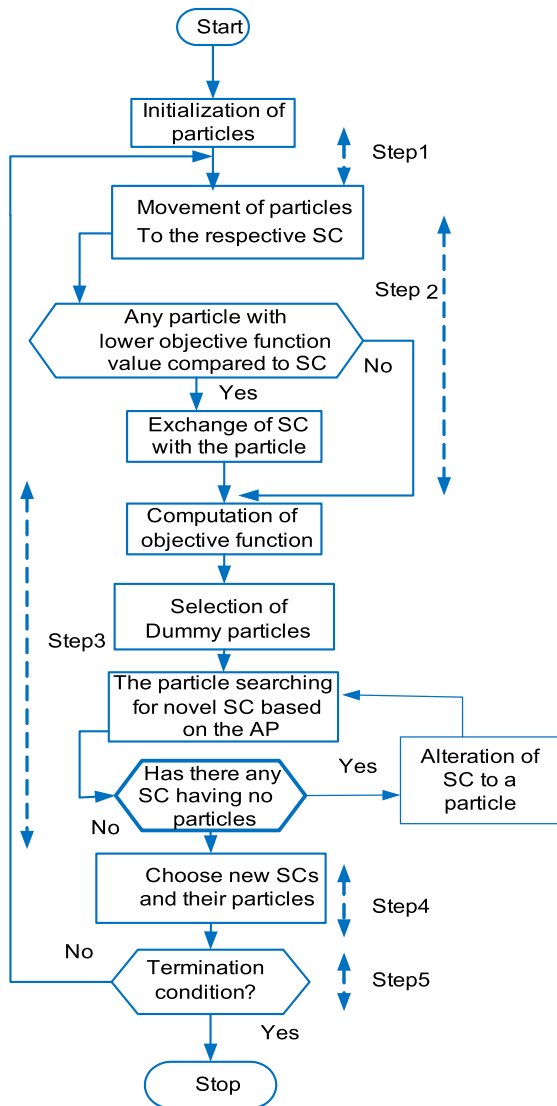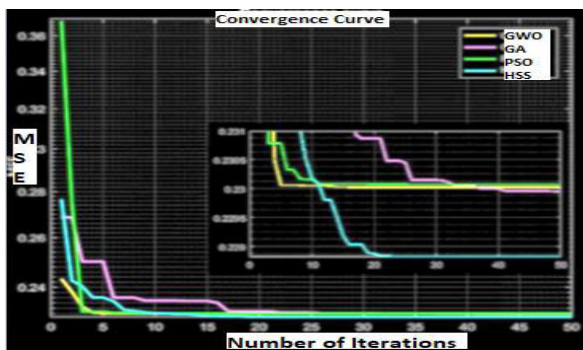
other conventional algorithms such as GWO,GA and PSO in the context of convergence rate and minimum fitness value. A higher convergence rate symbolises that a lower fitness value would be generated within a certain specified period. The convergence rate has been calculated with the mathematical formula

$$\frac{\sum_{n=1}^{N}(f_{n+1} - f_n)}{N}$$

f_n stands for the fitness of n-th evaluation and N is the total number of evaluations.

FIGURE 14. Flow chart of HSS algorithm.

FIGURE 15. Convergence Curve for GWO,GA,PSO and HSS algorithm.
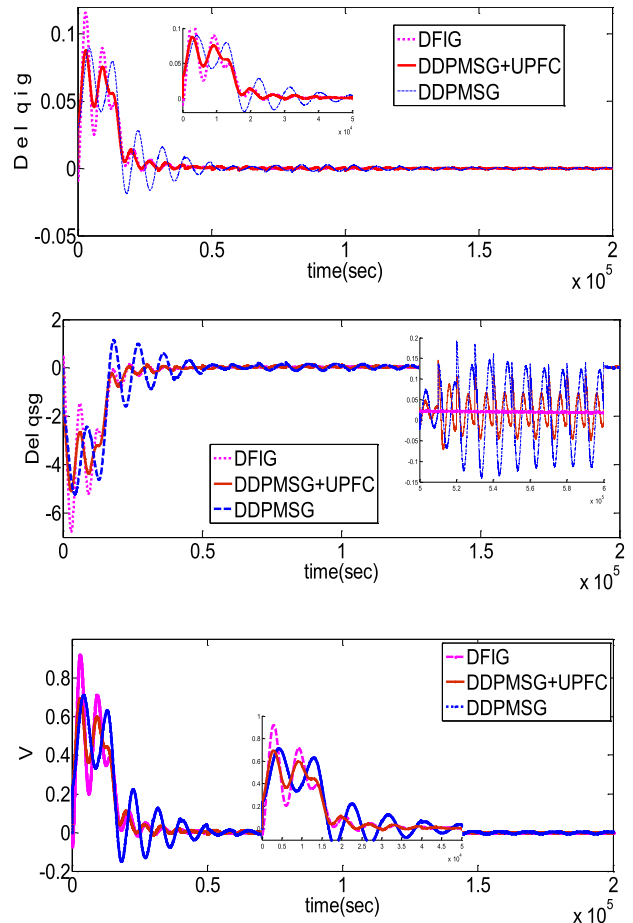

FIGURE 16. (a-c).Comparative results of UPFC based DDPMSG and DFIG.
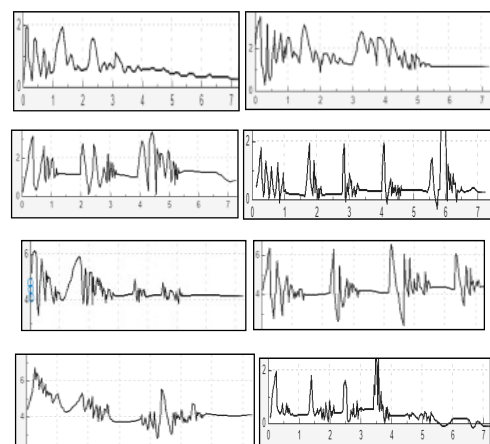
FIGURE 17. (a-h). Comparison of settling time of different parameters in the hybrid System.

determination of the stability plane is contingent upon the transfer function G(s), which serves as a representation of the transfer function of the HPS. The establishment of the

parameter K's range is of utmost importance in guaranteeing the stability of the Tidal diesel system. The proposed control strategy is designed to meet the requirements of this range, hence ensuring the system's stability. The value of K is constrained within the interval of negative infinity to 61.136. In addition, considering other significant stability

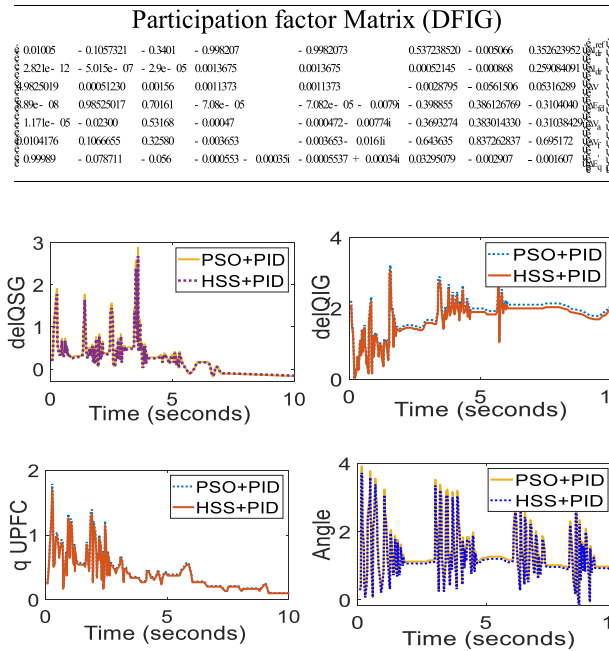**TABLE 4.** Comparison of participation factors of DFIG AND DDPMSG.

Participation factor Matrix (DFIG)							
0.01005	− 0.1057321	− 0.3401	− 0.9982207	− 0.9982073	0.537238520	− 0.005066	0.352623952
2.82e- 12	− 5.015e- 07	− 2.9e- 05	0.0013675	0.0013675	0.00052145	− 0.000868	0.259084091
0.9825019	0.00051230	0.00156	0.0011373	0.0011373	− 0.0028795	− 0.0561506	0.05316289
8.89e- 08	0.98525017	0.70161	− 7.08e- 05	− 7.082e- 05 − 0.0079i	− 0.398855	0.386126769	− 0.3104040
1.171e- 05	− 0.02300	0.53168	− 0.00047	− 0.000472- 0.00774i	− 0.3693274	0.383014330	− 0.310384292
0.0104176	0.1066655	0.32580	− 0.003653	− 0.003653- 0.016i	− 0.643635	0.837262837	− 0.695172
0.99989	− 0.078711	− 0.056	− 0.000553- 0.00035i	− 0.0005537 + 0.00034i	0.03295079	− 0.002907	− 0.001607

FIGURE 18. (a-d).Parameter outcome with random load inputs.
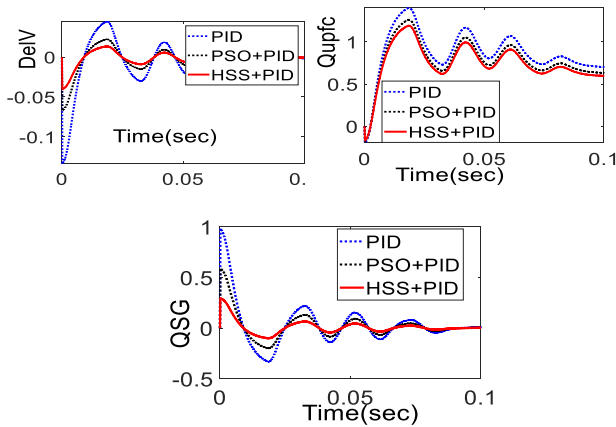
FIGURE 19. (a-c).Parameter outcome with PID,PSO+PID and HSS+PID based optimization.

FIGURE 20. (a-f). Stability analysis and performance with HSS based algorithm(a) eigen value plotting with DFIG(b) eigen value plotting with DDPMSG (c) Nyquist plotting (d) Box plots for with HSS Algorithm (e) Bode plotting (f)Popov criterion for stability analysis.

criteria such as Popov stability, the Popov line maintains an arbitrary orientation. The determination of Fmin and Fmax values occurs when the Popov line intersects the real axis. The research conducted by Circle and Popov provide valuable insights into the determination of the range of K and the sector boundary criteria pertaining to voltage stability.

Participation matrix indicates relationship in between selected state variables with that of the eigen values. Generally it represents the association between these right & left Eigen vectors.

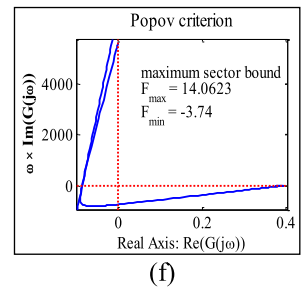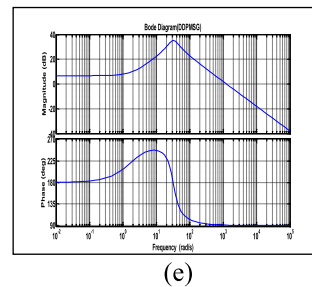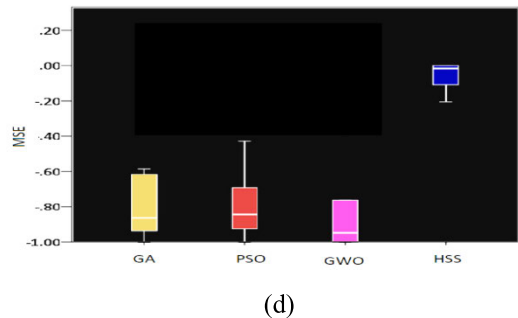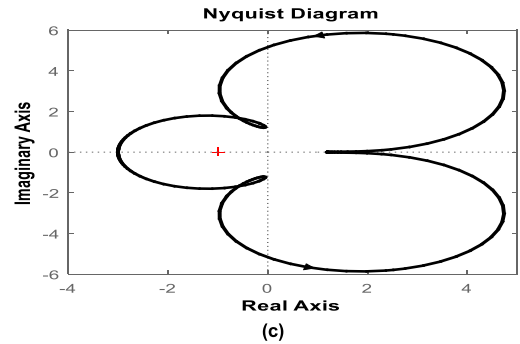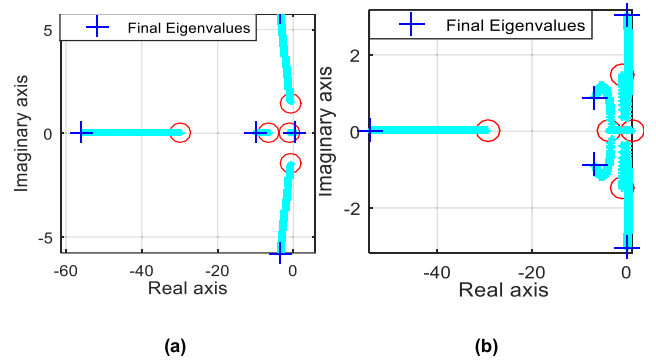$$[P] = [p1 \cdots\cdots\cdots\cdots pn] \qquad (15)$$

$$pi = \begin{bmatrix} p1i \\ p2i \\ . \\ . \\ . \\ pki \end{bmatrix} = \begin{bmatrix} f1i\varphi i1 \\ f2i\varphi i2 \\ . \\ . \\ . \\ fki\varphi ik \end{bmatrix} \qquad (16)$$

φ_{ki} indicates the k-th row and i-th column of the matrix$[\varphi]$.Eigen values give an indication about the stability
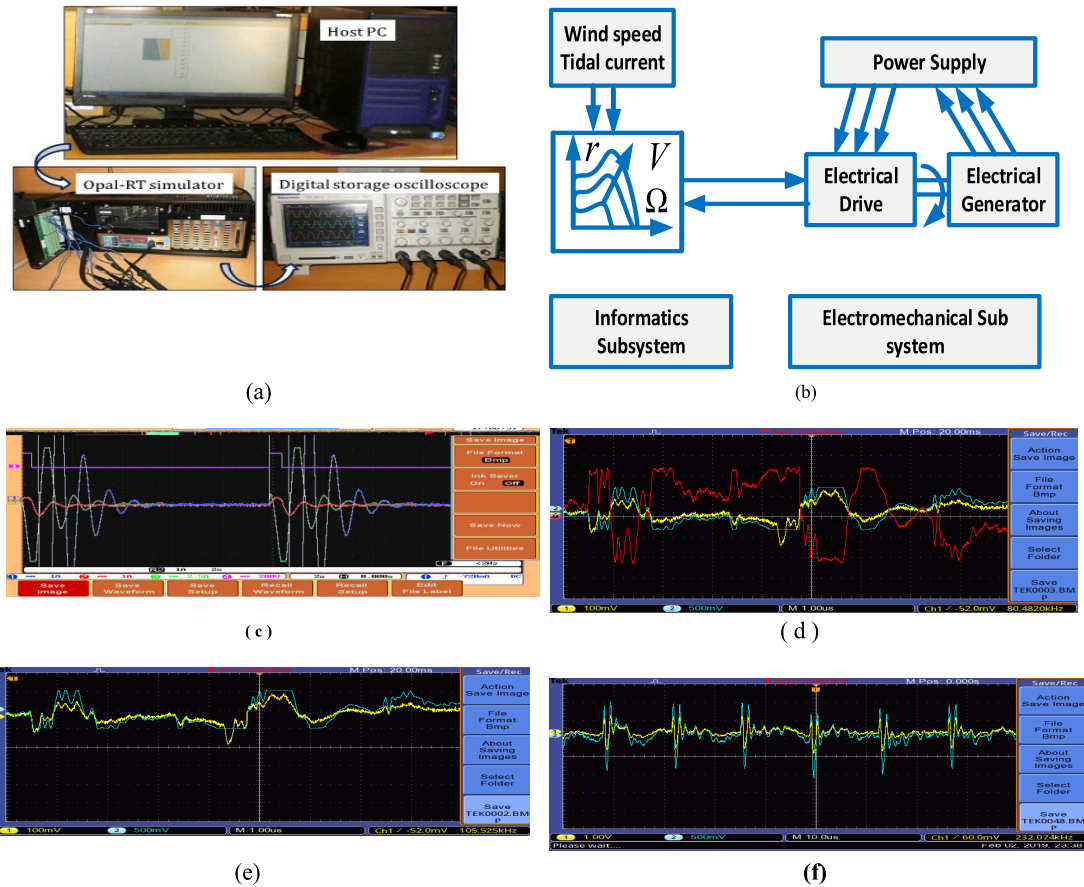
FIGURE 21. (a)The OP 5142 real-time digital simulator is utilized for conducting stability assessments. (b) A graphical representation illustrating the sequence and interconnection of hardware components involved in the loop simulation. (c) A visual depiction of the hardware configuration employed in the loop simulation.The graph displays the terminal voltage for different control strategies: Violet represents the load change strategy, Blue represents the PID strategy, Green represents the PSO-PID strategy, and Red represents the HSS-PID strategy. (d) This study investigates the performance of PID, PSO-PID, and HSS-PID control strategies under random load conditions. (e) The effects of a 5% change in load input on the performance of PSO-PID and HSS-PID control strategies are examined in this study. (f) The performance of PSO-PID and HSS-PID control strategies under repetitive loading conditions is evaluated in this study.

of Tidal based hybrid power system under load variation and uncertain Tidal power inputs.During observation it is found that eigen values remain on the left side of the imaginary axis of s plane. Eigen values in case of DDPMSG lie further left in compared to DFIG based Tidal HPS indicating enhancement of the damping as well as stability.

During the functioning of a real-time system, sensitivity analysis can be employed to evaluate the effect of abrupt changes (such as outages) on the system. Meanwhile, participation factors can aid in comprehending the contribution of specific generators or components to system variables.Sensitivity analysis can assist in fine-tuning control settings for best performance, while participation factors can direct control strategies by prioritizing essential components.

B. REAL-TIME SIMULATION STUDY IN OPAL-RT

To assess the validity of the suggested control approach and the efficacy of the corresponding system, a real-time simulation is conducted using the OPAL-RT 5142 simulator.

The findings of this simulation are presented and analyzed in the subsequent sub-section.Fig.18(a-b)This study aims to combine a digital storage oscilloscope and an OPAL-RT simulator into a Host PC running a 64-bit Windows 7 operating system with Xilinx v10.1 software. The multi-area power system is simulated using an OPAL-RT simulator, which is enhanced by the utilization of MATLAB 2011b version and distributed processing to improve computational speed. In addition, the Field-Programmable Gate Array (FPGA) module is integrated within the system, operating at a full-duplex rate of 2.6 gigabits per second. In addition, the Simulink model has been implemented on an FPGA within the RT-Lab real-time simulator. This was achieved through cluster programming in order to enhance its speed and enable distributed execution.

The aforementioned stages encompass the process of constructing the Simulink model and implementing recommended control techniques using s-functions available in MATLAB. The model is conducted with a load change of

5%, and the ensuing dynamic performance is illustrated in [Fig.18].Here violet line depicts the variations in load profile, whereas yellow, green as well as red curves illustrate the deviations in system terminal voltage when employing the traditional PID, PSO-PID, and HSS-PID methods, respectively[Fig.21] The utilization of an HSS optimized PID controller has been found to result in superior dynamic performance of the system, as seen by reduced settling time, overshoot, and undershoot in comparison with traditional controllers. Consequently, drawing upon the results elucidated in this investigation, one may deduce that the HSS-PID controller emerges as the most advantageous selection for the scrutinised power system owing to its remarkable aptitude for voltage regulation.

V. CONCLUSION

This paper discusses the stability and optimisation of Tidal HPS with Hyper Spherical Search (HSS) algorithm based UPFC controller.UPFC as a leading custom power device has improved the stability of Tidal system and established its robustness in reactive power management. Optimization and the System outcome at steady and transient state were analyzed through the HSS based algorithm. It can be summarized that the proposed HSS based DDPMSG system is more stable and parameters demonstrate better performances in terms of settling time,rise time,peak overshoot and damping as mentioned in Fig.2. HSS is compared to GA, PSO, and GWO to demonstrate its superiority in terms of both running time and convergence speed.The hybrid home energy system's optimal operating point is thoroughly examined and successfully attained, surpassing the findings of prior research that utilized GA, PSO, and GWO. The convergence curve is commonly considered the main qualitative indicator for evaluating the convergence performance of algorithms. Fig.15 illustrates the convergence curves, which represent the rate at which GWO, GA, PSO, and HSS converge in search spaces. Fig.15 demonstrates that the convergence curve of HSS displays a notably smoother and more rapid drop in comparison to GWO, GA, and PSO.

This approach is limited to selecting only continuous variables and cannot pick the features of specific subsystems using the continuous HSS technique. Thus, an additional discrete component will be incorporated and linked to this continuous process in order to choose the characteristic. If there is a combination of continuous and discrete variables, the search technique for the continuous component follows the method described in the continuous HSS, while the searching step for the discrete part is modified.

Further it includes a real time experimental analysis to validate the simulation results by the help of OPAL-RT Platform. The efficacy of the suggested controllers is assessed by stability analysis utilizing Eigen and Nyquist plots. The evaluation of the suggested control technique in the interconnected power system is performed utilising a real-time digital simulation platform called OPAL-RT 5142.

TABLE 5. Tidal based hybrid power system.

System Parameter Tidal based hybrid power System		Specification	
Tidal turbine Capacity		1.5 MVA	
Diesel power Capacity		1.5MVA	
Base Power capacity Load		2.5 MVA	
Synchronous Generator(SG)		2.5 MVA	
X'_d	0.29 pu	X_d	1.56 pu
T_e	0.55	δ (degree)	27.8
K_f	0.5	T_a	0.05
K_a	40	T'_{do}	4.49 sec
(DFIG)		P_{IN} in MVA	1.67
L_{SS}	3.07 pu	L_m	2.9 pu
Q_{DFIG}	0.125 pu	I_{dr}	0.4 pu
		$Q_L(pu)$	0.2
H_r	0.62 sec	T_S	0.08 sec

APPENDIX

A1-

$$f(x,y) = x\sin(4x) + 1.1y\sin(2y)$$
$$0 < X, Y > 10, MINIMUM : f(9.039, 8.668)$$

A2-

$$f(x,y) = 0.5 + \frac{\sin^2\sqrt{x^2+y^2} - 0.5}{1 + 0.1(x^2+y^2)}$$
$$-10 < x, y > 10, min : f(0,0) = 0$$

A3-

$$f(x,y) = -0.01e^{-0.2\sqrt{x^2+y^2}+3(\cos 2x + \sin 2y)}$$
$$-5 < x, y > 5, minimum : f(0,0) = 3.4536$$

A4-(De Jong's function)

$$f(x,y) = 0.1(x^2+y^2)$$
$$-10 < x, y > 10, min : f(0,0) = 0$$

A5-(Rosenbrock's valley function)

$$f(x,y) = 100(y-x^2)^2 + (1-x)^2$$
$$-10 < x, y > 10, minimum : f(0,0) = 0$$

A6-(Rastrigin's function):

$$f(x,y) = 0.1*\left(10*2 + \left(x^2 - 10\cos(2\pi x)\right) + \left(y^2 - 10\cos(2\pi y)\right)\right)$$

A7-(Griewangk's function):

$$f(x,y) = \frac{x^2+y^2}{4000} - \cos(x)\cos\left(\frac{y}{\sqrt{2}}\right) + 1$$
$$-10 < x, y > 10, min : f(0,0) = 0$$

REFERENCES

[1] I. M. Ducar and C. P. Ion, "Design of a PMSG for micro hydro power plants," in *Proc. 13th Int. Conf. Optim. Electr. Electron. Equip. (OPTIM)*, May 2012, pp. 712–717, doi: 10.1109/OPTIM.2012.6231949.

[2] C. E. Ugalde-Loo, L. A. Amézquita-Brooks, E. Licéaga-Castro, and J. Licéaga-Castro, "Analysis and efficient control design for generator-side converters of PMSG-based wind and tidal stream turbines," in *Proc. Power Syst. Comput. Conf.*, Aug. 2014, pp. 1–7, doi: 10.1109/PSCC.2014.7038495.

[3] D. Gautam and V. Vittal, "Impact of DFIG based wind turbine generators on transient and small signal stability of power systems," in *Proc. IEEE Power Energy Soc. Gen. Meeting*, Jul. 2009, p. 6551, doi: 10.1109/PES.2009.5275847.

[4] J. Yan, H. Lin, Y. Feng, and Z. Q. Zhu, "Control of a grid-connected direct-drive wind energy conversion system," *Renew. Energy*, vol. 66, pp. 371–380, Jun. 2014, doi: 10.1016/j.renene.2013.12.037.

[5] Y. Yasa and E. Mese, "Design and analysis of generator and converters for outer rotor direct drive gearless small-scale wind turbines," in *Proc. Int. Conf. Renew. Energy Res. Appl. (ICRERA)*, Oct. 2014, pp. 689–694, doi: 10.1109/ICRERA.2014.7016474.

[6] A. Mohanty, M. Viswavandya, S. Mohanty, and D. Mishra, "Fuzzy logic based UPFC controller for voltage stability and reactive control of a stand-alone hybrid system," in *Proc. 3rd Int. Conf. Adv. Comput., Netw. Inform.*, vol. 43, 2016, pp. 3–10, doi: 10.1007/978-81-322-2538-6_1.

[7] C. Qin and Y. Yu, "Small signal stability region of power systems with DFIG in injection space," *J. Modern Power Syst. Clean Energy*, vol. 1, no. 2, pp. 127–133, Sep. 2013, doi: 10.1007/s40565-013-0023-1.

[8] K. Ghefiri, S. Bouallègue, I. Garrido, A. Garrido, and J. Haggège, "Complementary power control for doubly fed induction generator-based tidal stream turbine generation plants," *Energies*, vol. 10, no. 7, p. 862, Jun. 2017, doi: 10.3390/en10070862.

[9] J. Zhao, X. Li, J. Hao, and J. Lu, "Reactive power control of wind farm made up with doubly fed induction generators in distribution system," *Electr. Power Syst. Res.*, vol. 80, no. 6, pp. 698–706, Jun. 2010, doi: 10.1016/j.epsr.2009.10.036.

[10] P. Ledesma and J. Usaola, "Doubly fed induction generator model for transient stability analysis," *IEEE Trans. Energy Convers.*, vol. 20, no. 2, pp. 388–397, Jun. 2005, doi: 10.1109/TEC.2005.845523.

[11] H. Polinder, F. F. A. van der Pijl, G.-J. de Vilder, and P. Tavner, "Comparison of direct-drive and geared generator concepts for wind turbines," in *Proc. IEEE Int. Conf. Electric Mach. Drives*, 2005, pp. 543–550, doi: 10.1109/IEMDC.2005.195776.

[12] H. Polinder, D. Bang, R. P. J. O. M. van Rooij, A. S. McDonald, and M. A. Mueller, "10 MW wind turbine direct-drive generator design with pitch or active speed stall control," in *Proc. IEEE Int. Electric Mach. Drives Conf.*, May 2007, pp. 1390–1395, doi: 10.1109/IEMDC.2007.383632.

[13] M. Noman, G. Li, K. Wang, and B. Han, "Electrical control strategy for an ocean energy conversion system," *Protection Control Modern Power Syst.*, vol. 6, no. 1, p. 18, Dec. 2021, doi: 10.1186/s41601-021-00186-y.

[14] J. Zhang, Z. Chen, and M. Cheng, "Design and comparison of a novel stator interior permanent magnet generator for direct-drive wind turbines," *IET Renew. Power Gener.*, vol. 1, no. 4, p. 203, 2007, doi: 10.1049/iet-rpg:20070054.

[15] A. Mohanty, M. Viswavandya, P. K. Ray, T. K. Panigrahi, and S. Mohanty, "Stability and optimisation of direct drive permanent magnet synchronous generator based tidal turbine," *Vacuum*, vol. 166, pp. 341–350, Aug. 2019, doi: 10.1016/j.vacuum.2018.10.052.

[16] A. Mohanty, M. Viswavandya, and S. Mohanty, "Prevention of transient instability and reactive power mismatch in a stand-alone wind-diesel-tidal hybrid system by an ANN based SVC," *Aquatic Proc.*, vol. 4, pp. 1529–1536, Sep. 2015, doi: 10.1016/j.aqpro.2015.02.198.

[17] Z. Tasneem, S. H. Rafi, and M. R. I. Sheikh, "Optimization of a direct-drive wind power generation system by using PMSG," in *Proc. Int. Conf. Electr. Eng. Inf. Commun. Technol. (ICEEICT)*, May 2015, pp. 1–5, doi: 10.1109/ICEEICT.2015.7307413.

[18] A. Mohanty, M. Viswavandya, S. Mohanty, and P. Paramita, "ANFIS-based controller for DFIG-based tidal current turbine to improve system stability," in *Proc. Int. Conf. Signal, Netw., Comput., Syst.*, in Lecture Notes in Electrical Engineering, 2016, pp. 115–122, doi: 10.1007/978-81-322-3589-7_12.

[19] S. Brisset, D. Vizireanu, and P. Brochet, "Design and optimization of a nine-phase axial-flux PM synchronous generator with concentrated winding for direct-drive wind turbine," *IEEE Trans. Ind. Appl.*, vol. 44, no. 3, pp. 707–715, Dec. 2008, doi: 10.1109/TIA.2008.921379.

[20] A. Sahoo and S. Chandra, "Multi-objective grey wolf optimizer for improved cervix lesion classification," *Appl. Soft Comput.*, vol. 52, pp. 64–80, Mar. 2017, doi: 10.1016/j.asoc.2016.12.022.

[21] M. H. Sulaiman, Z. Mustaffa, M. R. Mohamed, and O. Aliman, "Using the gray wolf optimizer for solving optimal reactive power dispatch problem," *Appl. Soft Comput.*, vol. 32, pp. 286–292, Jul. 2015, doi: 10.1016/j.asoc.2015.03.041.

[22] S. A. Ahmadi, H. Karami, M. J. Sanjari, H. Tarimoradi, and G. B. Gharehpetian, "Application of hyper-spherical search algorithm for optimal coordination of overcurrent relays considering different relay characteristics," *Int. J. Electr. Power Energy Syst.*, vol. 83, pp. 443–449, Dec. 2016, doi: 10.1016/j.ijepes.2016.04.042.

[23] D. Bertaccini, G. H. Golub, S. S. Capizzano, and C. T. Possio, "Preconditioned HSS methods for the solution of non-hermitian positive definite linear systems and applications to the discrete convection-diffusion equation," *Numerische Math.*, vol. 99, no. 3, pp. 441–484, Jan. 2005, doi: 10.1007/s00211-004-0574-1.

[24] Z.-Z. Bai and X. Yang, "On HSS-based iteration methods for weakly nonlinear systems," *Appl. Numer. Math.*, vol. 59, no. 12, pp. 2923–2936, Dec. 2009, doi: 10.1016/j.apnum.2009.06.005.

[25] Z.-Z. Bai and X.-P. Guo, "On Newton-HSS methods for systems of nonliear equations with positive-definite Jacobian matrices," *J. Comput. Math.*, vol. 28, no. 2, pp. 235–260, Jun. 2010, doi: 10.4208/jcm.2009.10-m2836.

[26] H. Karami, M. J. Sanjari, and G. B. Gharehpetian, "Hyper-spherical search (HSS) algorithm: A novel meta-heuristic algorithm to optimize nonlinear functions," *Neural Comput. Appl.*, vol. 25, no. 6, pp. 1455–1465, Nov. 2014, doi: 10.1007/s00521-014-1636-7.

[27] M. J. Sanjari, H. Karami, A. H. Yatim, and G. B. Gharehpetian, "Application of hyper-spherical search algorithm for optimal energy resources dispatch in residential microgrids," *Appl. Soft Comput.*, vol. 37, pp. 15–23, Dec. 2015, doi: 10.1016/j.asoc.2015.08.006.

[28] K. Eetivand, A. Zangeneh, and S. M. H. Nabavi, "Hyper-spherical search algorithm for maximum power point tracking of solar photovoltaic systems under partial shading conditions," *Int. Trans. Electr. Energy Syst.*, vol. 2022, pp. 1–18, Aug. 2022, doi: 10.1155/2022/1101692.

[29] M.-Z. Zhu, "Modified iteration methods based on the asymmetric HSS for weakly nonlinear systems," *J. Comput. Anal. Appl.*, vol. 15, no. 1, pp. 188–195, 2013.

[30] X.-P. Guo and I. S. Duff, "Semilocal and global convergence of the Newton-HSS method for systems of nonlinear equations," *Numer. Linear Algebra Appl.*, vol. 18, no. 3, pp. 299–315, May 2011.

ABHAY SANATAN SATAPATHY possesses extensive expertise in a variety of managerial roles. Throughout his career, he has held a number of positions with differing degrees of authority and responsibility. He is currently doing active research with the Faculty of Management Science, Sri Sri University, India. His areas of research are energy management in small scale industries, sustainability, and financial management strategy.

ASIT MOHANTY (Senior Member, IEEE) was graduated from NIT Durgapur. He is currently the Principal of MIET, Bhubaneswar. He has four long years of research experience with MNNIT Allahabad. He has more than 20 years of experience in teaching and research. He has published more than 150 technical articles in international conferences and refereed journals. His research interests include modeling and control of distributed energy sources, power system stability and control, power quality, and soft computing applications in power systems. He is a fellow of the Institute of Engineers, India; and a Life Member of the Indian Society for Technical Education (LMISTE).

PRAKASH K. RAY (Senior Member, IEEE) received the Ph.D. degree from MNNIT Allahabad, India, in 2012. He completed a postdoctoral fellowship with Nanyang Technological University (NTU), Singapore, in 2018. He is currently an Associate Professor with the Department of Electrical Engineering, OUTR, Bhubaneswar, India. He has published more than 200 technical papers in international conferences and refereed journals. His research interests include distributed generations, digital signal processing, and soft computing applications in power systems and power quality. He is a Life Member of the Indian Society for Technical Education (LMISTE).

AHMAD JABER MOHAMMAD ALFIAFI received the B.Sc. degree in engineering from the Department of Electrical Engineering. He is currently pursuing the master's degree with the Department of Electrical Engineering, King Khalid University, Abha, Saudi Arabia. His area of research interests include electric vehicles, power electronics, renewable energy, and electrical machines.

JAVED KHAN BHUTTO (Senior Member, IEEE) received the B.E. degree from Visvesvaraya Technological University (VTU), Belagavi, Karnataka, and the Master of Engineering degree in electrical engineering (power electronics, electrical machines, and drives) and the Ph.D. degree in engineering from the Malaviya National Institute of Technology (MNIT), Jaipur, Rajasthan, in the area of applications of power electronics in renewable energy. He has more than 18 years of teaching experience, exclusively in engineering colleges. Currently, he is an Associate Professor with the Department of Electrical Engineering, College of Engineering, King Khalid University, Abha, Saudi Arabia. He has authored two books in the field of electrical engineering and has contributed more than 30 technical papers on various topics in national and international journals and seminars. He is an Editorial Member of various journals (*IAEME*, *IJES*, *GRP*, *IAEE*, and *IJBER*).

OMAR KHULAIF ALHARBI (Member, IEEE) received the B.Sc. degree in engineering from the Department of Electrical Engineering, University of Hail, in 2018, and the master's degree from the Department of Electrical Engineering, King Khalid University, Abha, Saudi Arabia. His area of research are power electronics, renewable energy, and electrical machines.

• • •